BRAIN
ORIGINAL ARTICLE

# Structural (dys)connectivity associates with cholinergic cell density in Alzheimer's disease

Chen-Pei Lin,[1] Irene Frigerio,[1] Baayla D. C. Boon,[2,3] Zihan Zhou,[4] Annemieke J. M. Rozemuller,[2] Femke H. Bouwman,[3] Menno M. Schoonheim,[1] Wilma D. J. van de Berg[1] and Laura E. Jonkman[1]

Cognitive deficits in Alzheimer's disease, specifically amnestic (memory dominant) deficits, are associated with cholinergic degeneration in the basal forebrain. The cholinergic nucleus within the basal forebrain, the nucleus basalis of Meynert, exhibits local atrophy and reduced cortical tract integrity on MRI, and reveals amyloid-β and phosphorylated-tau pathology at autopsy. To understand the pathophysiology of nucleus basalis of Meynert atrophy and its neocortical projections in Alzheimer's disease, we used a combined post-mortem *in situ* MRI and histopathology approach. A total of 19 Alzheimer's disease (10 amnestic and nine non-amnestic) and nine non-neurological control donors underwent 3 T $T_1$-weighted MRI for anatomical delineation and volume assessment of the nucleus basalis of Meynert, and diffusion-weighted imaging for microstructural assessment of the nucleus and its projections. At subsequent brain autopsy, tissue dissection and immunohistochemistry were performed for amyloid-β, phosphorylated-tau and choline acetyltransferase. Compared to controls, we observed an MRI-derived volume reduction and altered microstructural integrity of the nucleus basalis of Meynert in Alzheimer's disease donors. Furthermore, decreased cholinergic cell density was associated with reduced integrity of the nucleus and its tracts to the temporal lobe, specifically to the temporal pole of the superior temporal gyrus, and the parahippocampal gyrus. Exploratory *post hoc* subgroup analyses indicated that cholinergic cell density could be associated with cortical tract alterations in amnestic Alzheimer's disease donors only. Our study illustrates that in Alzheimer's disease, cholinergic degeneration in the nucleus basalis of Meynert may contribute to damaged cortical projections, specifically to the temporal lobe, leading to cognitive deterioration.

1 Amsterdam UMC, Location VUmc, Vrije Universiteit Amsterdam, Department of Anatomy and Neurosciences, Amsterdam Neuroscience, Amsterdam, The Netherlands
2 Amsterdam UMC, location VUmc, Vrije Universiteit Amsterdam, Department of Pathology, Amsterdam Neuroscience, Amsterdam, The Netherlands
3 Amsterdam UMC, Location VUmc, Vrije Universiteit Amsterdam, Department of Neurology, Alzheimer centrum Amsterdam, Amsterdam, The Netherlands
4 Zhejiang University, College of Biomedical Engineering and Instrument Science, Zhejiang, China

Correspondence to: Chen-Pei Lin
De Boelelaan 1117
1081 HV, Amsterdam, The Netherlands
E-mail: c.p.lin@amsterdamumc.nl

Received August 06, 2021. Revised January 23, 2022. Accepted February 13, 2022.. Advance access publication March 8, 2022
© The Author(s) 2022. Published by Oxford University Press on behalf of the Guarantors of Brain.
This is an Open Access article distributed under the terms of the Creative Commons Attribution-NonCommercial License (https://creativecommons.org/licenses/by-nc/4.0/), which permits non-commercial re-use, distribution, and reproduction in any medium, provided the original work is properly cited. For commercial re-use, please contact journals.permissions@oup.com

Keywords: Alzheimer's disease; nucleus basalis of Meynert; cholinergic neurons; post-mortem diffusion MRI; histopathology

Abbreviations: CDR = Clinical Dementia Rating; ChAT = choline acetyltransferase; FA = fractional anisotropy; MD = mean diffusivity; NbM = nucleus basalis of Meynert; NFT = neurofibrillary tangle;

## Introduction

Alzheimer's disease is a heterogeneous disease characterized by memory deficits and cognitive decline with specific patterns of neurodegeneration. Clinically, a distinction can be made between an amnestic and non-amnestic subtype. In amnestic Alzheimer's disease, memory deficits are among the first symptoms, and in non-amnestic Alzheimer's disease, memory is initially spared, but symptoms of visuospatial impairment, aphasia or behavioural/dysexecutive dysfunction are more prominent.[1] Pathologically, Alzheimer's disease is characterized by abnormal aggregation of amyloid-β forming amyloid plaques, and phosphorylated-tau (p-tau) forming neurofibrillary tangles (NFTs).[2,3] Furthermore, one of the earliest sites of neurodegeneration is within the cholinergic nucleus basalis of Meynert (NbM), which is located in the substantia innominata of the basal forebrain.[4] Amyloid-β and NFT accumulation has been associated with cholinergic cell loss in the NbM, which in turn associated with decreased cortical acetylcholine and plays an important role in disease-related cognitive decline, specifically in memory and attention processing.[5–12] Imaging of the NbM has shown to be useful, for instance NbM volume can predict cognitive improvement after intake of galantamine, a common drug treatment targeting the cholinergic system in Alzheimer's disease.[13] Moreover, deep brain stimulation of the NbM is explored as a possible treatment option in Alzheimer's disease, by restoring the cholinergic transmission that is crucial in mediating memory processing.[14–16] It is therefore important to better understand the interplay between NbM protein aggregation, cholinergic cell loss, neuroimaging markers and cognition in Alzheimer's disease. This may help in evaluating and monitoring disease-related alterations, as well as therapeutic effects of cholinergic-targeting interventions.

*In vivo* MRI-measured volume of the NbM is thought to be sensitive to cholinergic degeneration, as illustrated by the decreased volume of the NbM in Alzheimer's disease patients compared to controls.[12,17,18] Moreover, recent advances in diffusion MRI measurements, specifically the fractional anisotropy (FA) and mean diffusivity (MD), allows us to not only examine the microstructural integrity within the NbM, but also the microstructural integrity of cholinergic projections.[19,20] Cholinergic projections to the frontal and temporal lobe were shown to be predominantly affected, and associate with cognitive dysfunctions.[21–24] Nevertheless, in these studies, the pathological substrate(s) underlying these MRI-measured alterations of the NbM and their cortical projections, were not explicitly addressed.

To this end, the current study investigated the associations between histopathological measures of cholinergic cell density, amyloid-β and p-tau, with within-subject post-mortem MRI-derived NbM volume, microstructural integrity and cortical projections, in Alzheimer's disease and non-neurological control donors. We hypothesized that, aside from volume and microstructural integrity of the NbM, its cortical projections, specifically to the frontal and temporal cortex, are affected and associate with pathological measures. In addition, due to the clinical and pathological heterogeneity in Alzheimer's disease, we explored the MRI and histopathological associations in clinically defined amnestic and non-amnestic subtypes, and hypothesized that the amnestic subtype is especially affected due to the cholinergic involvement in memory processing. The current study may lead to a better understanding of the pathophysiology underlying NbM atrophy and projections in *in vivo* imaging.

## Materials and methods

### Donor inclusion

A total of 28 brain donors, 19 Alzheimer's disease and nine non-neurological control donors, were included in the study, with written informed consent for the use of their brain tissue and medical records for research purposes. Alzheimer's disease donors were included in collaboration with the Alzheimer centre Amsterdam and the Netherlands Brain Bank (http://brainbank.nl). During life, patients were screened according to the screening protocol of the Amsterdam Dementia Cohort.[25] Diagnosis was made by a multidisciplinary team according to NINCDS-ADRDA criteria.[26] The overall score on the five-point Clinical Dementia Rating (CDR) scale was used to stage global dementia severity around the time of death and is reported when available.[27] An Alzheimer's disease subtype distinction could be made between amnestic ($n = 10$) patients, and non-amnestic ($n = 9$) patients according to the IWG-2 criteria,[28] with the latter one being subdivided into six patients clinically diagnosed with the behavioural/dysexecutive and three patients with posterior cortical atrophy.[28,29] Non-neurological controls included at the Department of Anatomy and Neurosciences, Amsterdam UMC, location VUmc, following the Normal Aging Brain Collection Amsterdam (NABCA; http://nabca.eu) pipeline.[30] Donors were excluded if any of the following criteria applied: (i) cause of death due to neurological or mental disorder, including sepsis, encephalitis, asphyxia, a cerebrovascular accident or traumatic brain injury; (ii) with medical history of neurological or psychiatry diagnosis; or (iii) with presence of neurological abnormalities at *in situ* post-mortem MRI or neuropathological change at post-mortem pathological assessments. Neuropathological diagnosis of all donors was confirmed by an expert neuropathologist (A.J.M.R.) and performed according to the international guidelines of the Brain Net Europe II (BNE) consortium (http://www.brainneteurope.org). All donors underwent post-mortem *in situ* MRI and brain autopsy. The study design is summarized in Fig.1.

### Post-mortem *in situ* and ante-mortem MRI acquisition

Post-mortem MRI data were acquired by whole-brain *in situ* (brain still in cranium) scanning on a whole-body 3 T MR scanner (Signa-MR750, General Electric Medical Systems) with an eight-channel phased-array head-coil.[30] $T_1$-weighted images were acquired using a sagittal 3D $T_1$-weighted fast spoiled gradient echo sequence with the following parameters: repetition time (TR)/echo time (TE)/inversion time (TI) = 7/3/450 ms, flip angle = 15°, slice thickness = 1 mm, in-plane resolution = $1.0 \times 1.0$ mm$^2$. A sagittal 3D fluid attenuation inversion recovery (FLAIR) was acquired with TR/TE/TI = 8000/130/2000–2250 ms, slice thickness 1.2 mm, in-plane resolution = $1.11 \times 1.11$ mm$^2$. In addition, the

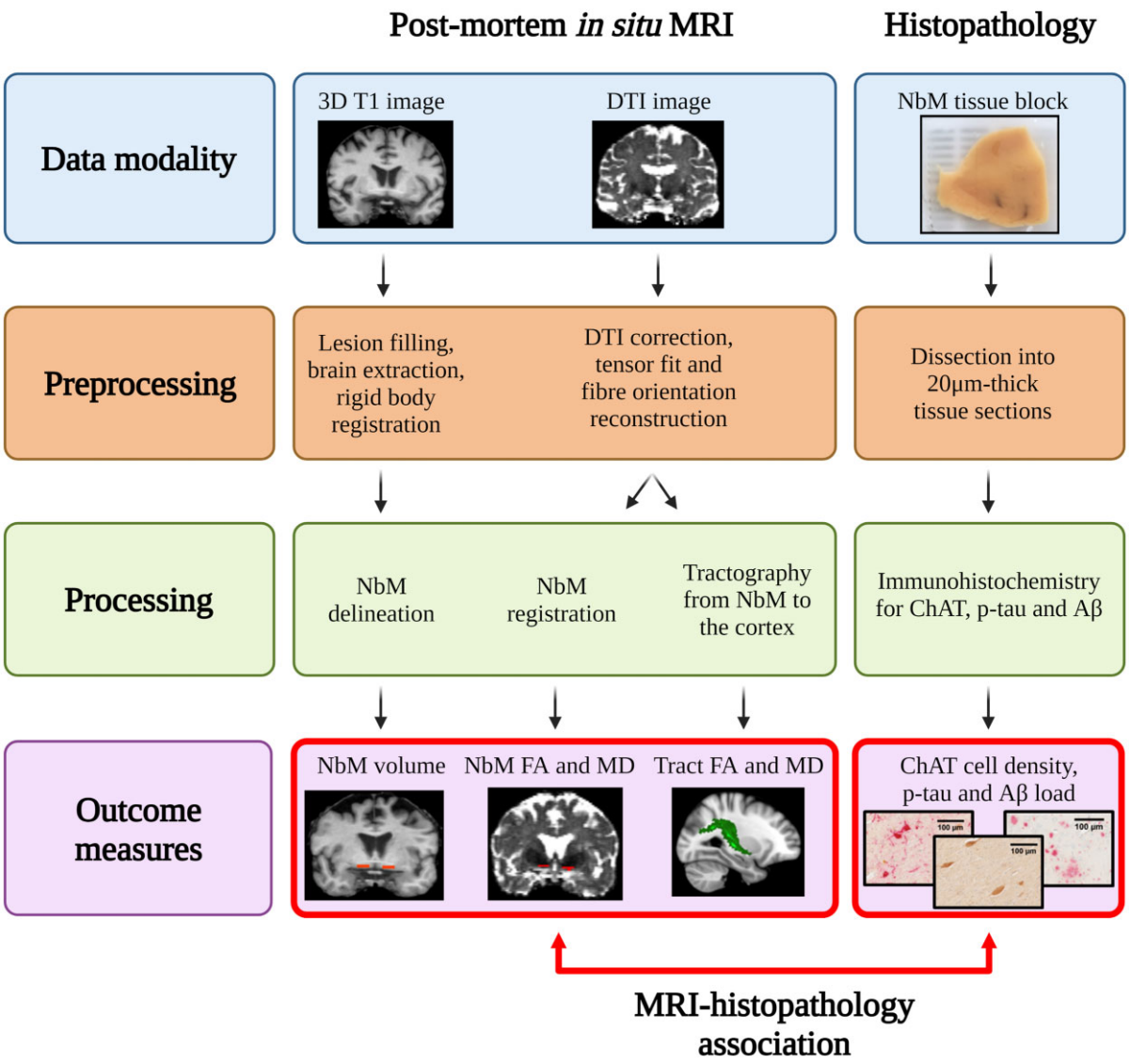


**Figure 1 Study design of combined post-mortem *in situ* MRI and histopathology.** The figure illustrates the (pre)processing steps of MRI and histopathological data, and the outcome measures in the current study. The red double-headed arrow indicates the associative statistical analysis between MRI and histopathological outcome measures. Aβ = amyloid-beta; DTI = diffusion tensor images; p-tau = phosphorylated-tau.

inversion time (TI) of the FLAIR sequence was optimized per case to account for variable CSF suppression due to post-mortem delay. Diffusion-weighted imaging (DWI) was acquired by axial 2D echo-planar imaging with diffusion gradients applied in 30 non-collinear directions, TR/TE = 7400/92 ms, slice thickness 2.0 mm, in-plane resolution = 2.0 × 2.0 $mm^2$ and $b$ = 1000 $s/mm^2$. To allow for offline distortion correction of the images, FIVE b0 images were acquired using the same sequence parameters. Ante-mortem MRI data were retrospectively obtained from the Amsterdam Dementia Cohort with similar parameters to the post-mortem MRI sequence, as previously described.[25,31]

## MRI analysis

### Structural image processing

To minimize the impact of age-related white matter abnormalities (e.g. vascular change) on automated segmentations, the 3D $T_1$ images were lesion-filled,[32] as previously described,[33] Subsequently, normalized brain volumes of the whole brain, white matter and grey matter were estimated from 3D $T_1$ images using SIENAX,[34] FMRIB Software Library (FSL) tools version 5.0.9 (https://fsl.fmrib.ox.ac.uk/fsl/). In addition, each hemisphere was parcellated into 39 anatomical regions using the automated anatomical labelling atlas,[35] and transformed from 3D $T_1$ to diffusion space using boundary-based registration and FMRIB's Integrated Registration and Segmentation Tool for further diffusion analysis.

### NbM delineation on MRI

3D $T_1$ images were registered to MNI orientation using an affine rigid-body transformation. In this standardized orientation, the NbM was delineated (both left and right hemisphere) in each subject, using five consecutive coronal sections of 1 mm, based on the method described previously.[36–38] In brief, the first delineating section was identified at the level of crossing anterior commissure. The dorsal border of the NbM aligned with the most ventral aspect

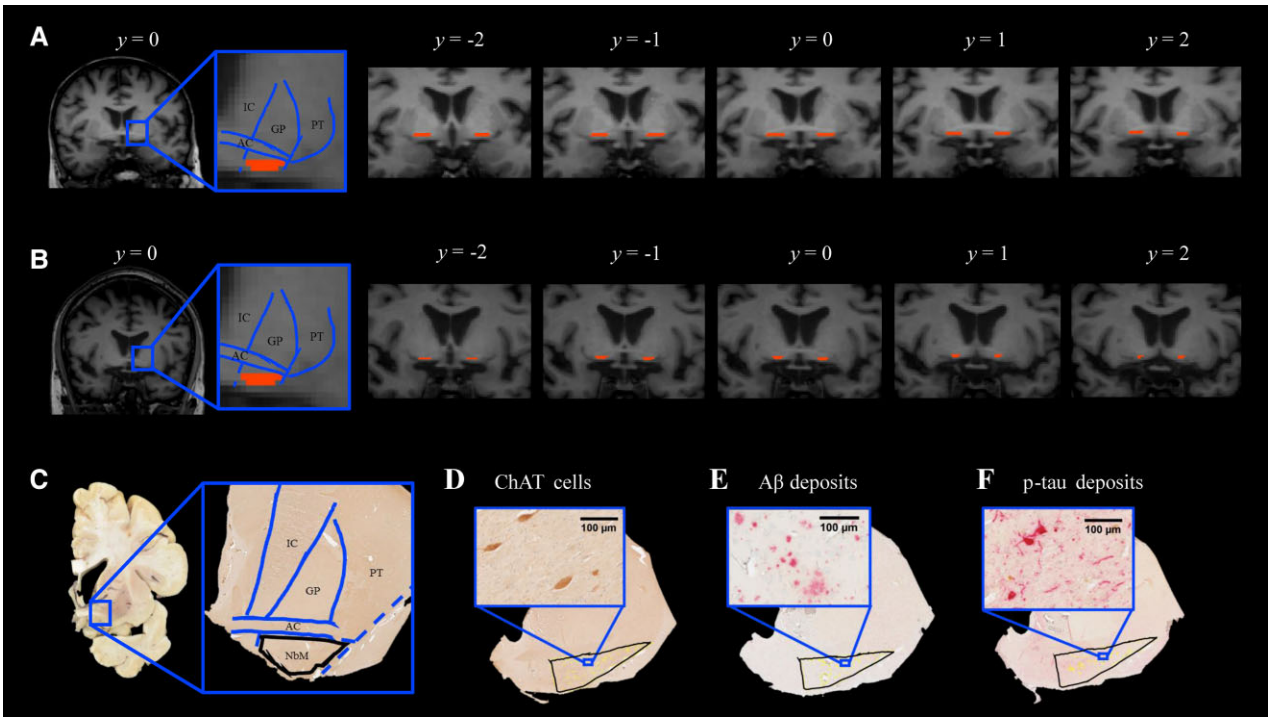


**Figure 2 NbM delineation in MRI $T_1$ coronal scans and histological sections.** Illustration of NbM delineation in five consecutive $T_1$ coronal images of a control (**A**) and an Alzheimer's disease donor (**B**). On the image with the highest signal intensity of visible anterior commissure (AC), denoted as y = 0, the NbM was delineated according to the standard guideline based on anatomical landmarks of the AC, internal capsule (IC), globus pallidus (GP), putamen (PT). Subsequently, the NbM was delineated on two adjacent images forwards and backwards (y = –2 to y = 2). (**C**) Illustration of NbM delineation in histological sections of a control. Delineation was performed primarily on ChAT single stained sections, with illustrated standard guidelines based on the same anatomical landmarks as in **A**. In an Alzheimer's disease donor, the delineated NbM exhibits ChAT immunoreactivity with visible ChAT cells in **D**, amyloid-β deposit in **E** and p-tau deposit in **F** with visible p-tau tangles and threads. Aβ = amyloid-beta; p-tau = phosphorylated-tau.

of the globus pallidus, while the ventral border of the NbM was the final row of voxels before the csf. The lateral border of NbM was delineated along the medial aspect of the putamen, whereas the medial border was demarcated following the extended ventrolateral outline of the internal capsule to the base of the brain (Fig. 2A and B). The NbM delineation was performed by C.L. The intra-rater variability was determined on a subset of 19 cases with the intraclass correlation coefficient of 0.76, which is considered excellent agreement.[39] Furthermore, the inter-rater variability was determined between the delineation of C.-P.L. and an independent rater, N.R., on a subset of 14 cases. The inter-rater intraclass correlation coefficient was 0.58, which is considered moderate to good agreement.[39] Left and right NbM volumes were calculated and normalized for head size using the V-scaling factor from SIENAX. Subsequently, the NbM was reversely transformed to native 3D $T_1$ space, and coregistered to diffusion space using boundary-based registration parameters.

## DTI processing

DTI was first corrected for eddy current induced geometric distortion and fitted for diffusion tensors.[40,41] Subsequently, diffusion orientation distributions were modelled using FDT (part of FSL 5.0.9). The delineated NbM was overlaid onto the FA and MD diffusion maps to derive the FA and MD values of the NbM.[42] Tracts between the NbM and cortical atlas regions were determined using probabilistic tractography. For this, BEDPOSTX, a function from FDT, was used to model the distribution of fibre orientations at each voxel yielding the voxel-wise diffusion orientations for performing probabilistic tractography.

## Probabilistic tractography

Probabilistic tractography was performed using ProbTrackX2 (FDT, FSL 5.0.9) with default settings and 5000 sampling fibres. The cortical tracts were reconstructed in each hemisphere separately with left or right NbM as seed regions of interest. Subsequently, tracts were binarized and FA and MD of tracts were calculated by overlaying the tracts onto the diffusion maps. In a stepwise fashion, to limit the number of comparisons, we first addressed tracts from the NbM to the cingulum and cortical lobes (frontal, temporal, parietal, occipital cortex and insula)[43]; see Supplementary Table 1 for a list of composite automated anatomical labelling regions. For tracts that showed significant associations between FA or MD and pathological measures, we subsequently addressed the integrity of tracts to the subregions of these cortical lobes (e.g. superior, middle and inferior temporal gyrus; Supplementary Table 1). The diffusion measures were corrected for the volume of the seed region, the NbM, to control for effects of volume variation on tractography FA and MD.

## NbM tissue sampling, processing and quantification

After post-mortem *in situ* MRI, the donors were transported to the mortuary for brain autopsy. According to the standard protocol, after the brain was extracted from cranium, the left hemisphere was instantly dissected and preserved for molecular and

biochemistry analysis (and therefore not used in the current study), whereas the right hemisphere was fixed in 4% formalin for 4 weeks and subsequently dissected for paraffin embedding and (immuno) histochemical analysis.[30,44] Tissue blocks were retrospectively collected from each case. Based on the Dickson sampling scheme,[45] tissue blocks with visible substantia innominata that contains the NbM were sampled in a corona plane where the substantia innominata was visible underneath the anterior commissure at the level of the caudate-putamen. The blocks were subsequently paraffin embedded, followed by immunohistochemistry.

### Immunohistochemistry for cholinergic neurons, amyloid-β and p-tau

For detailed methods, see the Supplementary material. In brief, paraffin-embedded tissue NbM blocks were cut at 20 µm for 30 consecutive sections and stained for single choline acetyltransferase (ChAT) and double ChAT/Aβ (6F/3D) and ChAT/p-tau (AT8). From the first section with visible anterior commissure and substantia innominata, three sections with a distance of 200 µm in between were included per staining. To assess the effect of cortical Alzheimer's disease pathology on cholinergic innervation, paraffin-embedded tissue blocks of the parahippocampal gyrus were cut at 6 µm and stained for amyloid-β (4G8) and p-tau (AT8). The primary antibodies used for each staining are shown in Supplementary Table 2. Finally, ChAT was visualized with 3,3′-diaminovenzidine (DAB, Dako) imidazole, whereas p-tau and amyloid-β were visualized using liquid permanent red followed by counterstaining with haematoxylin, and mounted with Entellan.

### NbM delineation on tissue sections

Tissue sections of four Alzheimer's disease cases had to be excluded due to incorrect anatomical orientation or tissue disintegration during the staining process. Immunostained sections were digitally scanned with the Vectra Polaris Quantitative Pathology Imaging System (PerkinElmer, USA) at ×20 magnification. The NbM was manually delineated on the ChAT-stained sections using Fiji ImageJ v.1.52r (https://imagej.nih.gov/ij), which was subsequently used as template for delineation in the ChAT/p-tau and ChAT/Aβ double stained sections (Fig. 2C–F). Based on previous literature,[4,46,47] the region of interest for NbM was defined independent of the cholinergic cells, but according to the anatomical landmarks of neighbouring structures so that the disease-related cholinergic loss would not affect the selected area. Similar to the MRI delineation, the ventral aspect of the anterior commissure serves as the dorsal border, whereas the base of the brain serves as the ventral border of the region of interest. The lateral border was delineated following the ventrolateral outline of the global pallidus that intersects the anterior commissure and further extends to the base of the brain, while the medial border aligns the extended lateral outline of internal capsule to the base of the brain. To account for the heterogeneous distribution of cholinergic cells within NbM, the sections were further subdivided into 'pre-anterior', 'anteroromediate' and 'antero-intermediate' NbM on the basis of the emergence of anterior commissure and neighbouring anatomical structures and visualized in Supplementary Fig. 1.[4,8,47–49] The sections were denoted as 'pre-anterior NbM' if the ChAT cells were underneath the visible and continuous anterior commissure that is ventral to the globus pallidus and rostral to decussation level. The sections were denoted as 'anteroromediate NbM' if the ChAT cells were underneath or adjacent to the elongated and continuous anterior commissure. The sections were denoted as 'antero-intermediate NbM' if the ChAT cells were underneath or adjacent to the tip of the rostral anterior commissure and underneath the putamen. As these subsectors were unevenly distributed in the Alzheimer's disease and control group, this distinction is included as a covariate in the statistical analysis.

### Quantification of cholinergic cell density and pathological load

After region of interest delineation, ChAT, amyloid-β and p-tau were quantified using in-house ImageJ scripts. For ChAT cell density, circular objects with a size between 20 and 200 µm in diameter were selected and ChAT cell count per $mm^2$ was calculated. For amyloid-β and the p-tau, the load (%area) showing immunopositive signal within the region of interest was calculated (Supplementary Fig. 2). All derived measures were averaged across the three sections for each immunostaining. In summary, our immunohistochemical outcome measures after averaging across three sections were ChAT cell density, amyloid-β load and p-tau load.

### Statistical analysis

Statistical analysis was performed using IBM SPSS 22.0 for Windows (SPSS, Inc., Chicago, IL, USA). All the statistical variables were tested for normality. Non-normally distributed data were log transformed, including FA, MD, ChAT cell density, amyloid-β and p-tau load. The Chi-square test was used to investigate group difference between Alzheimer's disease donors and non-neurological controls, and between Alzheimer's disease subtypes (amnestic and non-amnestic) for categorical variables, e.g. gender and pathological staging. General linear models were used for the aforementioned group differences in MRI-derived outcome measures (NbM volume, FA and MD, as well as FA and MD of tracts to the cortex), and histopathological outcome measures (ChAT cell density, amyloid-β and p-tau load). We applied Spearman's correlation, partial correlations and linear mixed models to examine the associations between the previously mentioned MRI and histopathology-derived outcome measures within the right hemisphere, as well as the associations between MRI outcome measures and CDR scores. Only the MRI outcome measures of the right hemisphere was used to associate with histopathological measures because the histopathology was only assessed in the right hemisphere, as previously mentioned. We further evaluate the effect size of our statistical outcomes, deriving the Cohen's *d* and correlation coefficients *r*. Age, gender and post-mortem delay were included as covariates in all statistical analysis.[50] The NbM subsectors, as mentioned in a previous paragraph, were included as covariate in statistical analysis of ChAT cell density. NbM volume was included as covariate in statistical analysis of NbM tracts.[51] All data were corrected for multiple comparisons with Bonferroni correction and false discovery rate (FDR).[52]

### Data availability

The data that support the findings of this study are available from the corresponding author on reasonable request.

## Results

### Study cohort

Clinical, neuropathological and radiological characteristics of each group are shown in Table 1, and details of each donor are shown in

**Table 1 Clinical, radiological and pathological characteristics of donors**

| | Controls | Alzheimer's disease |
|---|---|---|
| **Clinical and cognitive characteristics** | | |
| *n* | 9 | 19 |
| Gender female/male (% male) | 4/5 (56%) | 4/15 (79%) |
| Age at death, years, mean ± SD | 70.8 ± 8.8 | 67.4 ± 11.6 |
| Disease duration, years, mean ± SD | — | 8.1 ± 4.8 |
| Dutch education (level), *n* | NA | 17 |
| 0/1/2/3/4/5/6/7 | | 0/0/1/0/2/3/5/6 |
| CDR, *n* | NA | 17 |
| 0/1/2/3 | | 0/5/4/8 |
| PMD, mean (h:min) ± SD (h) | 9:10 ± 3 | 7:23 ± 2 |
| **Radiological characteristics** | | |
| NBV (l), mean ± SD | 1.46 ± 0.07 | 1.41 ± 0.13 |
| NWMV (l), mean ± SD | 0.70 ± 0.04 | 0.73 ± 0.08 |
| NGMV (l), mean ± SD | 0.79 ± 0.04 | 0.67 ± 0.09* |
| **Pathological and genetic characteristics** | | |
| Thal phase, *n* | 9 | 19*** |
| 0/1/2/3/4/5 | 2/3/3/1/0/0 | 0/0/0/1/1/17 |
| Braak NFT stage, *n* | 9 | 19*** |
| 0/1/2/3/4/5/6 | 1/7/1/0/0/0/0 | 0/0/0/0/4/8/7 |
| ABC score, *n* | 9 | 19 |
| A 0/1/2/3 | 2/6/1/0 | 0/0/0/19*** |
| B 0/1/2/3 | 1/8/0/0 | 0/0/4/15*** |
| C 0/1/2/3 | 9/0/0/0 | 0/0/4/15*** |
| APOE genotype, *n* | 8 | 19 |
| ϵ4 non-carrier | 5 (56%) | 7 (37%) |
| ϵ4 heterozygous | 3 (44%) | 10 (53%) |
| ϵ4 homozygous | 0 | 2 (10%) |

*n* = sample size; NA = not available; NBV = normalized brain volume; NGMV = normalized grey matter volume; NWMV = normalized white matter volume; PMD = post-mortem delay; SD = standard deviation.

*$P < 0.05$, compared to controls.

***$P < 0.001$, compared to controls.

Supplementary Table 3. There were no significant differences in age and post-mortem delay between Alzheimer's disease donors and controls, however, the Alzheimer's disease group had more males than the control group ($P = 0.02$). Normalized total brain volume and normalized white matter volume were comparable between groups. As expected, the Alzheimer's disease donors had lower normalized grey matter volume ($P = 0.046$), higher Braak NFT stages ($P < 0.001$),[2] Thal phases ($P < 0.001$)[53] and ABC scores ($P < 0.001$)[54] than controls, while APOE genotype did not differ between groups ($P = 0.453$).

## NbM volume, microstructure and tracts

Both left and right normalized NbM volumes were lower in Alzheimer's disease donors compared to controls ($P = 0.027$ and $P = 0.036$, respectively, Fig. 3A). To illustrate that post-mortem *in situ* NbM volume is comparable to *in vivo* NbM volume, we obtained ante-mortem NbM volume of five Alzheimer's disease patients, of which three were acquired within a year before death, and two were 8–10 years before death. The NbM volumes obtained from scans with short intervals were similar to the post-mortem NbM volumes, with an average volume difference of 15.20 $mm^3$. The volumes obtained from scans with longer intervals were more discrepant to the post-mortem NbM volumes, with an average volume difference of 81.85 $mm^3$ (Supplementary Table 4).

Right FA ($P = 0.069$) and left MD ($P = 0.478$) of the NbM were comparable between groups, but both left NbM FA ($P = 0.047$, $d = 2.11$) and right MD ($P = 0.030$, $d = 2.36$) were higher in Alzheimer's disease donors compared to controls (Fig. 3B and C). Correlations were found between NbM volume and NbM MD in the right ($r = -0.60$, $P = 0.001$), but not left hemisphere ($P = 0.236$) (Fig. 3D and E and Supplementary Table 5).

Alzheimer's disease donors did not show differential NbM tract integrity (FA or MD) to cortical lobes compared to controls (Supplementary Table 6). In the right hemisphere, decreased NbM volume was associated with reduced microstructural integrity of the NbM tract to the temporal lobe (FA: $r = 0.52$, $P = 0.048$, FDR corrected, MD: $r = -0.58$, $P = 0.018$, FDR corrected), but not to other cortical or cingulate areas (Supplementary Table 5).

## NbM associations with neuropathological stages

Reduced NbM volume was correlated with higher Braak NFT stages ($r = -0.44$, $P = 0.029$). However, no correlations were found between NbM microstructural integrity (FA or MD) and Braak NFT stage or Thal phase (all $P > 0.05$).

## NbM pathological load and ChAT cell density

Alzheimer's disease donors showed higher pathology load (%area) of amyloid-β ($P = 0.002$) and p-tau ($P < 0.001$) than controls (Supplementary Table 7). No significant difference in ChAT cell density was observed between groups ($P = 0.384$). This is most likely due to the large variability in both groups, particularly in the Alzheimer's disease group (Fig. 4). ChAT cell density was not associated with local amyloid-β ($P = 0.467$) or p-tau load ($P = 0.871$).

## ChAT cell density associates with MD of the NbM and its tracts to the temporal cortex

When assessing MRI and histopathological associations in the whole cohort, MRI-derived NbM MD correlated negatively with ChAT cell density ($r = -0.49$, $P = 0.028$), but not with amyloid-β and p-tau load ($P = 0.670$ and $P = 0.249$, respectively). NbM volume and FA did not associate with ChAT cell density, amyloid-β, and p-tau load (all $P > 0.05$). (Supplementary Table 8).

When considering the microstructural integrity of tracts between the NbM and cortical lobes, ChAT cell density was negatively associated with MD of tracts to the temporal lobe ($r = -0.70$, $P = 0.024$, FDR corrected), while no associations were found in other cortical tracts (Fig. 5A and Supplementary Table 9). When excluding one control case exhibiting especially high ChAT cell density (90.186 count per $mm^2$, falling outside the inner quartile), the association did not survive correction for multiple comparisons ($r = -0.62$, $P = 0.011$, uncorrected; $P = 0.064$, FDR corrected). No significant associations were found between NbM tract integrity and amyloid-β, and p-tau load. Association estimates and *P*-values of tracts to cingulate and cortical lobes are shown in Supplementary Table 9.

## ChAT cell density associates with MD of tracts to the temporal pole and parahippocampal gyrus

These results indicate specific alterations in the tracts to the temporal lobe, of which the decreased tract MD was associated with reduced ChAT cell density. To explore this further, we investigated

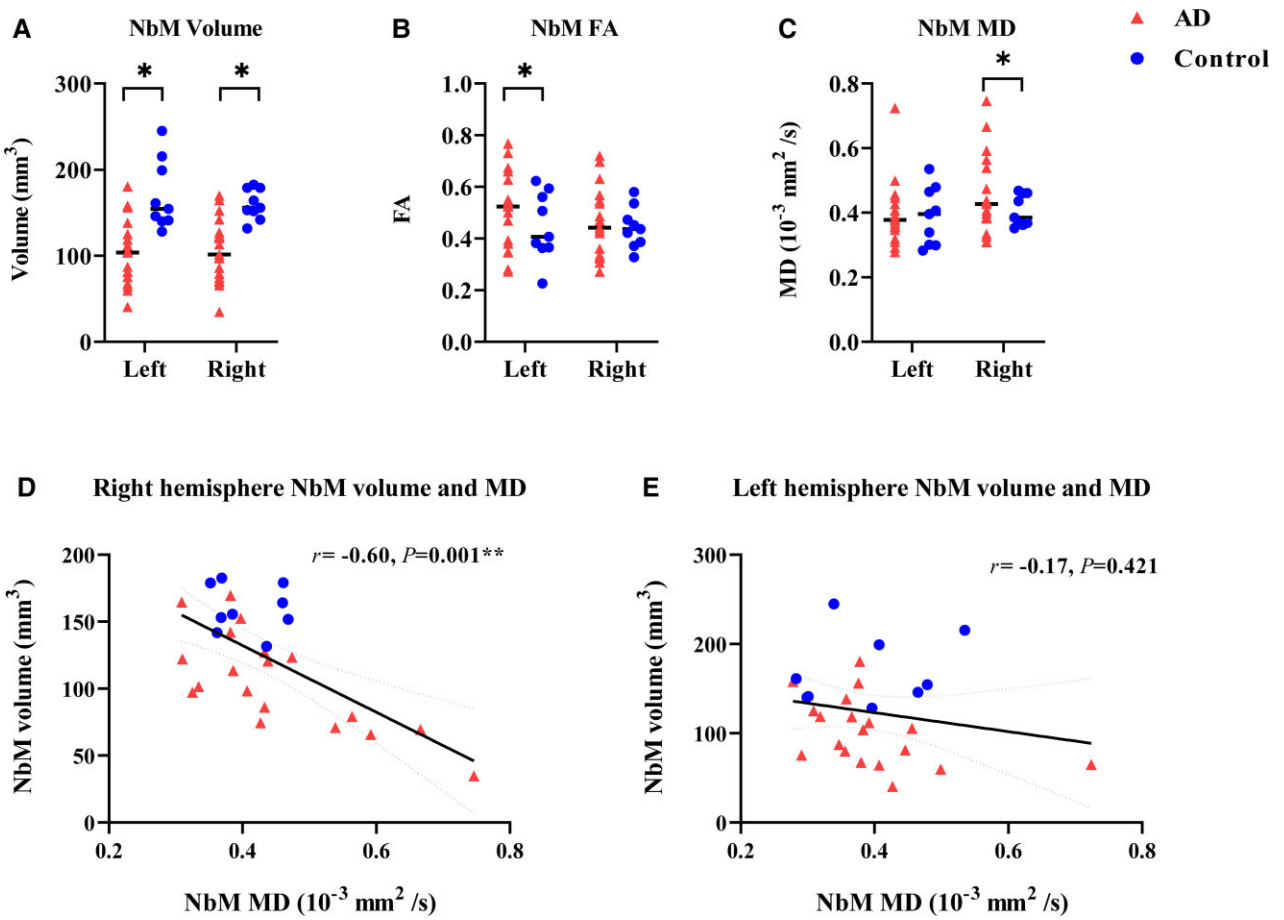


**Figure 3 MRI measures of NbM volume, microstructure and their associations.** Alzheimer's disease cases showed significantly lower NbM volumes in the left ($P = 0.027$) and right ($P = 0.036$) hemispheres in **A**, higher FA in NbM of the left hemisphere ($P = 0.047$) in **B** and higher NbM MD in the right hemisphere ($P = 0.030$) in **C** compared to controls. The NbM volumes significantly correlated with the NbM MD in the right hemisphere ($P = 0.001$), as shown in **D**; however, no significant correlation was found for the left hemisphere ($P = 0.421$), as shown in **E**. For detailed information, see Supplementary Table 5. AD = Alzheimer's disease; $r$ = rho. $^{*}P < 0.05$. $^{**}P < 0.01$.

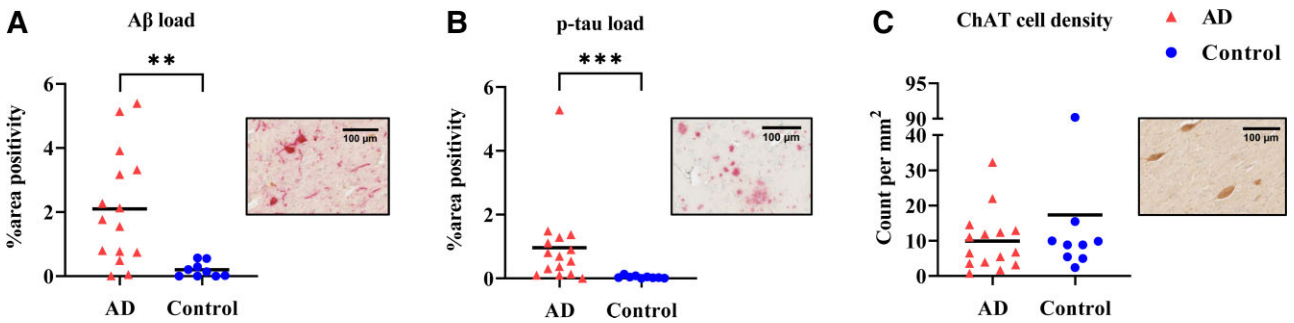


**Figure 4 Alzheimer's disease cases showed higher pathological load in the NbM but not lower ChAT cell density compared to controls.** Alzheimer's disease donors had significantly higher amyloid-β ($P = 0.002$) and p-tau ($P = 0.0002$) load as shown in **A** and **B**. However, ChAT cell density did not differ to controls, as shown in **C**. Of note, some Alzheimer's disease donors had very little ChAT cell density, while others had similar counts to controls, illustrating the heterogeneity in our Alzheimer's disease cohort. Pathology inserts show the immunoreactivity of amyloid-β (Aβ) (**A**), p-tau (**B**) and ChAT (**C**). AD = Alzheimer's disease; p-tau = phosphorylated-tau. $^{**}P < 0.01$. $^{***}P < 0.001$.

the tracts to subdivisions of the temporal cortex. As such, ChAT cell density was negatively associated with MD of the tracts to the middle temporal gyrus ($r = -0.55$, $P = 0.049$, FDR corrected), temporal pole of superior temporal gyrus ($r = -0.92$, $P < 0.001$, FDR corrected), temporal pole of middle temporal gyrus ($r = -0.52$, $P = 0.049$, FDR corrected) and parahippocampal gyrus ($r = -0.80$, $P = 0.003$, FDR corrected), as shown in Table 2. When excluding the aforementioned outlier case, the associations between ChAT cell density and tract MD remained significant in tracts to the temporal pole of the superior temporal gyrus and parahippocampal gyrus (respectively $r = -0.80$, $P = 0.003$ and $r = -0.71$, $P = 0.016$, FDR corrected) (Fig.5).

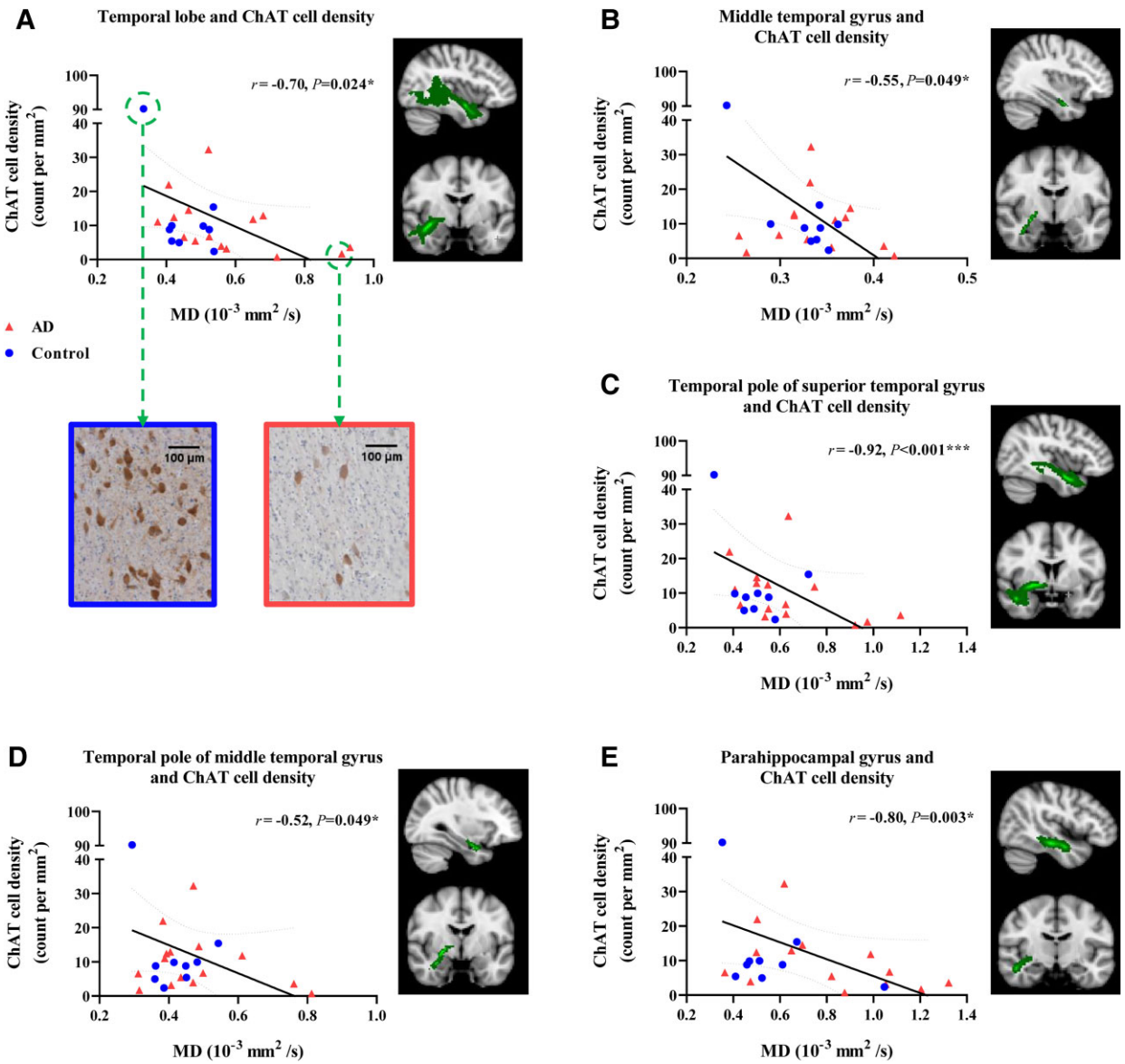


**Figure 5 ChAT cell density associated with MD of tracts to the temporal lobe and subregions.** ChAT cell density was negatively associated with MD of tracts to temporal lobe, as shown in **A**. Pathology *insets* show a control case with high ChAT cell density exhibiting low tract MD, and an Alzheimer's disease case with low ChAT cell density exhibiting high tract MD. Negative associations were also found between ChAT cell density and MD of tracts to temporal subregions: middle temporal gyrus (**B**), temporal pole of superior and middle temporal gyrus (**C**) and (**D**), and parahippocampal gyrus (**E**). After removal of a case with very high ChAT cell density, the associations remained for temporal pole of superior temporal gyrus ($r = -0.80$, $P = 0.003$, FDR corrected) and parahippocampal gyrus ($r = -0.71$, $P = 0.016$, FDR corrected). AD = Alzheimer's disease. *$P < 0.05$, FDR corrected. **$P < 0.01$, FDR corrected, ***$P < 0.001$, FDR corrected.

**Table 2 Associations between ChAT cell density and the integrity of tracts to regions within the temporal lobe**

| | Superior temporal gyrus | Middle temporal gyrus | Inferior temporal gyrus | Temporal pole, superior temporal gyrus | Temporal pole, middle temporal gyrus | Parahippocampal gyrus | Hippocampus |
|---|---|---|---|---|---|---|---|
| **Tract FA** | | | | | | | |
| ChAT cell density | P = 0.883 | P = 0.391 | P = 0.872 | P = 0.124 | P = 0.872 | r = 0.70<br>P = 0.027* | P = 0.872 |
| **Tract MD** | | | | | | | |
| ChAT cell density | P = 0.191 | r = −0.55<br>P = 0.049* | r = −0.51<br>P = 0.053 | r = −0.92<br>P < 0.001*** | r = −0.52<br>P = 0.049* | r = −0.80<br>P = 0.003** | P = 0.349 |

*$P < 0.05$, FDR corrected.
**$P < 0.01$, FDR corrected.
***$P < 0.001$, FDR corrected.

### Amyloid-β load in the parahippocampal gyrus associates with parahippocampal tract MD

To investigate the role of reduced tract integrity between the NbM and parahippocampal gyrus on neocortical protein accumulation, we associated amyloid-β and p-tau load in the parahippocampal gyrus with parahippocampal tract MD. We found that increased parahippocampal amyloid-β load was associated with decreased parahippocampal tract MD ($r = –0.51$, $P = 0.025$). However, no association was found between p-tau load and parahippocampal tract MD ($P = 0.087$).

### Correlations with CDR scores

To address cholinergic integrity in relation to dementia severity, we examined the correlations between the integrity of the NbM and its projections with the CDR score in Alzheimer's disease donors. Increased NbM MD was correlated with a higher CDR score ($r = 0.56$, $P = 0.036$), whereas no correlations were found for NbM volume or FA (respectively, $P = 0.191$ and $P = 0.499$). A negative trend was found in the correlation between MD of the NbM tract to the temporal lobe ($r = 0.67$, $P = 0.052$, FDR corrected). Within the temporal lobe, increased MD of the tracts to the superior temporal gyrus ($r = 0.78$, $P = 0.036$, FDR corrected) and parahippocampal gyrus ($r = 0.80$, $P = 0.006$, FDR corrected) were correlated with a higher CDR score.

In addition, a higher CDR score is correlated with reduced ChAT cell density ($r = –0.69$, $P = 0.029$) and increased amyloid-β load ($r = –0.76$, $P = 0.011$), but not p-tau load ($P = 0.547$) within the NbM.

### Exploration in Alzheimer's disease subtypes

Our Alzheimer's disease cohort contained amnestic and non-amnestic clinical subtypes; due to this heterogeneity we explored a possible phenotypic effect in our results. Supplementary Table 10 shows the clinical, neuropathological and radiological characteristics of the phenotypes. No significant differences in these characteristics were found between the two subtypes, but both subtypes showed differences compared to controls.

MRI-derived volume of both left and right NbM were lower in the amnestic subtype compared to controls (left: $P = 0.018$, and right: $P = 0.029$, uncorrected), but no difference between the non-amnestic subtype and controls, as well as between the two subtypes was found. Only tracts between the NbM and temporal lobe showed higher FA in amnestic compared to non-amnestic subtype ($P = 0.036$, Bonferroni-corrected).

For histopathological measures, both subtypes had higher p-tau load than controls (amnestic: $P = 0.001$, and non-amnestic: $P = 0.018$, Bonferroni-corrected), while only the amnestic subtype had higher amyloid-β load than controls ($P = 0.006$, Bonferroni-corrected). No significant difference in p-tau load, amyloid-β load or ChAT cell density was found between subtypes (Supplementary Table 11).

When examining MRI-histopathology associations in the amnestic subtype, positive associations were found between p-tau load and MRI-derived NbM volume ($r = 0.75$, $P = 0.032$), p-tau load and the FA of NbM tracts to the temporal lobe ($r = 0.89$, $P = 0.018$, FDR corrected), whereas negative associations were found between ChAT cell density and MD of tracts between the NbM and frontal, temporal and parietal lobes (respectively, $r = –0.89$, $P = 0.024$; $r = –0.89$, $P = 0.018$; $r = –0.79$, $P = 0.040$, FDR corrected). In contrast, we did not find any MRI-histopathology associations in non-amnestic subtype (Supplementary Table 12).

## Discussion

In a combined post-mortem *in situ* MRI and histopathology approach, we investigated the associations between MRI-derived NbM volume, microstructure and tractography with NbM protein aggregation and cholinergic cell density, in Alzheimer's disease and non-neurological control donors. We found reduced NbM microstructural integrity to be associated with decreased cholinergic cell density, and higher dementia scores. Furthermore, this decrease in the cholinergic cell density in the NbM was associated with altered integrity in white matter tracts between the NbM and regions within the temporal cortex. Interestingly, this was specifically the case for amnestic rather than non-amnestic Alzheimer's disease donors.

In our study, post-mortem NbM MRI volume loss was found in Alzheimer's disease compared to control donors, which has also been described previously in the *in vivo* literature.[12,55] We did not find a group difference in the integrity of tracts between the NbM and the frontal and temporal lobe. Although not previously addressed in *in vivo* neuroimaging studies, histological studies have shown disrupted cholinergic pathways and cholinergic denervation to the frontal and temporal lobe in Alzheimer's disease.[56,57] The reason why we did not find such differences may be due to the heterogeneity of our Alzheimer's disease cohort, as we did find differences in the integrity of the tract between the NbM and temporal cortex between amnestic and non-amnestic subtypes. We also showed that NbM atrophy was associated with local decreased microstructural integrity, similar to the association found in an *in vivo* MRI study in Alzheimer's disease.[18] Moreover, we found increased NbM MD to be associated with lower cholinergic cell density, and higher CDR scores in Alzheimer's disease donors, suggesting that MRI-derived MD may be a sensitive marker for cholinergic degeneration and cognitive deterioration in Alzheimer's disease.[58–62]

We did not find an absolute reduction in cholinergic cell density in Alzheimer's disease compared to control donors, a finding that is both consistent and contradictory to the literature.[6,9,63–65] It is suggested that these inconsistent results reflect the large heterogeneity in cholinergic cell loss within subsectors of the NbM.[4] There appears to be a caudorostral gradient of NbM neuronal loss in Alzheimer's disease, with the posterior sector being the most severely affected.[4,9,66,67] We identified our tissue sections as part of the pre-anterior/anteroromediate/antero-intermediate NbM,[4,47,49] which could explain why we did not find a group difference in cholinergic cell density.

Although NbM amyloid-β and p-tau load were higher in Alzheimer's disease than control donors, they were not correlated with NbM MRI outcome measures. This is in line with literature showing no correlation between local amyloid-plaque or NFT load with MRI-measured NbM volume.[68] However, we did find an association between NbM volume and Braak NFT stages, corroborating an *in vivo* study associating NbM volume and CSF p-tau levels.[69] This may suggest a closer relationship between NbM alterations with cortical pathology rather than local pathological burden. Nevertheless, local NbM pathological burden may be involved in altered NbM integrity in specific Alzheimer's disease phenotype(s), as we found an association between NbM volume and p-tau in amnestic, rather than non-amnestic, Alzheimer's disease donors. However, these associations were made with a very small sample size, therefore results should be interpreted with caution and should be further explored in a larger cohort with a variety of phenotypes.[1,47]

We found decreased ChAT cell density associated with an increased MD of tracts to the temporal lobe, specifically to the

temporal pole of superior temporal gyrus and parahippocampal gyrus, suggesting that the effects of cholinergic degeneration on cholinergic pathways can be captured with diffusion MRI. The lateral cholinergic pathways of the NbM innervates the superior, middle and inferior temporal gyrus and parahippocampal gyrus, and is responsible for cortical cholinergic signalling in the temporal lobe.[22,70] Cholinergic denervation may lead to reduced acetylcholine in the medial temporal cortex, and decrease spiking activity in cholinergic neurons, which in turn decreases activation of cholinergic receptors, undermining memory formation in Alzheimer's disease.[10,24,71–73] Specifically, parahippocampal acetylcholine activity plays a role in mediating memory encoding and consolidation.[71,74] This shows the crucial role of temporal cholinergic projections in supporting memory-related circuitry in the medial temporal lobe, which is clinically relevant in amnestic Alzheimer's disease.[13,14,75]

Interestingly, the MRI-measured parahippocampal tract integrity also associated with amyloid-β burden within the parahippocampal gyrus. Indeed, previous animal studies showed that cholinergic lesions in the basal forebrain, or direct removal of cholinergic innervation, induced deposition of amyloid-β-related pathology in the cortex, and later on behavioural deficits in memory performance.[76–79] In our results, we found that reduced parahippocampal tract integrity associated with increased amyloid-β burden, and higher CDR scores in Alzheimer's disease donors. Altogether, suggesting that cholinergic degeneration in the NbM, and alterations in its tracts, may induce abnormal cortical cholinergic signalling, affecting cognitive performance.

The cholinergic system is differentially affected in clinically defined Alzheimer's disease subtypes.[80] Memory deficits in amnestic Alzheimer's disease have been linked to cholinergic dysfunction,[6] whereas symptoms of non-amnestic Alzheimer's disease, such as visual hallucination and aphasia, have been linked with focal pathological change in specific brain areas.[81,82] We explored the cholinergic integrity among the subtypes in our cohort and found cholinergic alterations only within the amnestic subtype. Compared to controls, MRI-derived volume reduction and higher pathological burden was found in the NbM of amnestic donors, while no difference was shown in the non-amnestic donors. Furthermore, decreased ChAT cell density was associated with increased MD of tracts between the NbM and frontal, temporal and parietal lobes only within amnestic Alzheimer's disease donors. Altogether, cholinergic transmission to the neocortex may be predominantly interrupted in the amnestic subtype, as illustrated by altered integrity in NbM tracts and memory-related symptoms. Moreover, p-tau accumulation in the NbM may play a role in this cholinergic disruption, especially to the temporal lobe.[83]

Of note, we only found tract MD, and not FA, to be associated with the histopathological outcome measures. MD has been shown to be more sensitive in characterizing microstructural change in Alzheimer's disease due to its intrinsic biophysical properties. It describes the average directional diffusivity, directly reflecting the expansion or narrowing of extracellular space under the change of either one or more diffusivities.[60,84] On the other hand, FA is a function of axial and radial diffusivity, which therefore remains constant when both directional diffusivities change proportionally to each other.[85] Previous studies have shown that MD, as well as the radial diffusivity, were able to detect extensive abnormalities in major white matter bundles in Alzheimer's disease.[84,86] In addition, white matter MD, rather than FA, has been shown to correlate with abnormal CSF $A\beta_{1-42}$ and CSF tau level in early stage Alzheimer's disease,[59] and more significantly with pathological staging and cognitive outcomes.[87] We cannot, however, rule out technical interference that might dilute the effects of FA. A recent study using free water-corrected FA, yielded a correlation with cortical amyloid-β burden, specifically entorhinal tau burden in PET.[88] As such, MD seems to be most sensitive for pathological alterations in Alzheimer's disease at present, while the sensitivity of FA may require further research and more optimized methodological strategies.

More bridging evidence between neuroimaging and histopathology is needed to support our results and further validate and identify useful imaging (bio)markers and potential post-treatment auxiliary in Alzheimer's disease.[89–91] A few limitations of our study need to be addressed. First, regardless of the scientific benefit of *in situ* MRI, the post-mortem setting does not reflect the *in vivo* situation in absolute terms. Increased FA and reduced MD have been reported due to a drop in body temperature after death.[92,93] However, these measures are altered linearly across ante- and post-mortem white matter pathways.[94] Therefore, taking post-mortem delay as a covariate in our analysis, relative comparisons can be made. Second, our small sample size along with the heterogeneity in Alzheimer's disease group, requires replication and further validation in a larger cohort to better account for the clinical and pathological heterogeneity, and to be able to differentiate cholinergic projections to cortical subregions in Alzheimer's disease phenotypes. The use of an atlas-based NbM template is also recommended to minimize intra-/inter-rater variability and reduce labour intensity in manual delineation.[18] In addition, our NbM tissue blocks were retrospectively collected from the brain bank and not directly at the autopsy where the dissecting plain for the NbM block can be derived more consistently across cases to reduce the variability in NbM subsectors. Apart from projecting to the cortical lobes, the NbM also projects to the amygdala, having an important role in learning and memory in Alzheimer's disease.[95] Due to its anatomical location, visualization of this particular pathway remains difficult. A higher resolution, or multi-shell DWI, could help to reduce crossing fibre issues to better reconstruct these white matter tracts.[96]

Other than the NbM, also referred to as Ch4 region, the basal forebrain cholinergic system encompasses the Ch1-3 regions, located at the medial aspect of the basal forebrain.[4,97] *In vivo* MRI studies have shown atrophy of these regions associated with cognitive decline and pathological Thal phases in Alzheimer's disease.[68,75] While Ch1-2 projects to the hippocampus,[4,97] atrophy has been shown in both the Ch1-2 and hippocampus in those with mild cognitive impairment.[17] As Ch1-2 tissue was unavailable in this study, further research is needed to disentangle the distinctive roles of other basal forebrain cholinergic subregions and their projections, as well as the underlying pathological substrates.[98] Furthermore, recent studies have also raised attention to co-morbid pathology in Alzheimer's disease, such as TAR DNA-binding protein 43 and Lewy body pathology.[99,100] Future research is encouraged to account for alternative secondary pathologies to better understand the pathological mechanisms underlying cholinergic degeneration in Alzheimer's disease and related disorders.

In conclusion, the present study investigated cholinergic degeneration within the NbM and its structural projections to cortical regions with combined post-mortem MRI and histopathology. Alzheimer's disease donors showed reduced NbM volume and altered NbM integrity. In addition, the decline in cholinergic cell density was associated with microstructural alterations in the NbM and its projections, specifically to the temporal cortex, and correlated with the severity of cognitive impairment. Together, these findings indicate that pathological alterations in the

cholinergic system in Alzheimer's disease are not limited to the NbM, but can also be captured in its cortical projections, potentially in patients with an amnestic phenotype. As such, the current study reveals an association between MRI and histopathology of the cholinergic system in Alzheimer's disease, which provides valuable insights in the pathophysiology underlying *in vivo* imaging (bio)markers.

## Acknowledgements

We would like to thank all brain donors and their caregivers for deciding to donate their brains to research, as well as the Netherlands Brain Bank and the Normal Aging Brain Collection Amsterdam (NABCA) autopsy teams. Special thanks to Niels Reijner (N.R.) who assisted with the MRI delineation.

## Funding

This study was funded by Alzheimer's Association (Research Fellowship AARF-18-566459), Zon M.W. Memorabel (grant no. 733050102) and Michael J. Fox (Grant ID 17253).

## Competing interests

The authors report no competing interests.

## Supplementary material

Supplementary material is available at *Brain* online.

## References

1. Graff-Radford J, Yong KXX, Apostolova LG, *et al*. New insights into atypical Alzheimer's disease in the era of biomarkers. *Lancet Neurol*. 2021;20:222–234.
2. Braak H, Braak E. Neuropathological stageing of Alzheimer-related changes. *Acta Neuropathol*. 1991;82:239–259.
3. Selkoe DJ. Amyloid β protein precursor and the pathogenesis of Alzheimer's disease. *Cell*. 1989;58:611–612.
4. Liu AKL, Chang RCC, Pearce RKB, Gentleman SM. Nucleus basalis of Meynert revisited: Anatomy, history and differential involvement in Alzheimer's and Parkinson's disease. *Acta Neuropathol*. 2015;129:527–540.
5. Arendt T, Bigl V, Arendt A, Tennstedt A. Loss of neurons in the nucleus basalis of Meynert in Alzheimer's disease, paralysis agitans and Korsakoff's disease. *Acta Neuropathol*. 1983;61:101–108.
6. Whitehouse PJ, Price DL, Struble RG, Clark AW, Coyle JT, DeLong MR. Alzheimer's disease and senile dementia: Loss of neurons in the basal forebrain. *Science*. 1982;215:1237–1239.
7. Mesulam M, Shaw P, Mash D, Weintraub S. Cholinergic nucleus basalis tauopathy emerges early in the aging-MCI-AD continuum. *Ann Neurol*. 2004;55:815–828.
8. Mesulam MM, Geula C. Nucleus basalis (Ch4) and cortical cholinergic innervation in the human brain: Observations based on the distribution of acetylcholinesterase and choline acetyltransferase. *J Comp Neurol*. 1988;275:216–240.
9. Iraizoz I, Guijarro JL, Gonzalo LM, De Lacalle S. Neuropathological changes in the nucleus basalis correlate with clinical measures of dementia. *Acta Neuropathol*. 1999;98:186–196.
10. Haense C, Kalbe E, Herholz K, *et al*. Cholinergic system function and cognition in mild cognitive impairment. *Neurobiol Aging*. 2012;33:867–877.
11. Hampel H, Mesulam MM, Cuello AC, *et al*. The cholinergic system in the pathophysiology and treatment of Alzheimer's disease. *Brain*. 2018;141:1917–1933.
12. Grothe M, Heinsen H, Teipel SJ. Atrophy of the cholinergic basal forebrain over the adult age range and in early stages of Alzheimer's disease. *Biol Psychiatry*. 2012;71:805–813.
13. Müller P, Vellage AK, Schmicker M, *et al*. Structural MRI of the basal forebrain as predictor of cognitive response to galantamine in healthy older adults: A randomized controlled double-blinded crossover study. *Alzheimers Dement*. 2021;7:e12153.
14. Yu D, Yan H, Zhou J, Yang X, Lu Y, Han Y. A circuit view of deep brain stimulation in Alzheimer's disease and the possible mechanisms. *Mol Neurodegener*. 2019;14:33.
15. Kumbhare D, Palys V, Toms J, *et al*. Nucleus basalis of Meynert stimulation for dementia: Theoretical and technical considerations. *Front Neurosci*. 2018;12:614.
16. Gratwicke J, Kahan J, Zrinzo L, *et al*. The nucleus basalis of Meynert: A new target for deep brain stimulation in dementia? *Neurosci Biobehav Rev*. 2013;37:2676–2688.
17. Cantero JL, Zaborszky L, Atienza M. Volume loss of the nucleus basalis of Meynert is associated with atrophy of innervated regions in mild cognitive impairment. *Cereb Cortex*. 2017;27:3881–3889.
18. Teipel SJ, Flatz WH, Heinsen H, *et al*. Measurement of basal forebrain atrophy in Alzheimer's disease using MRI. *Brain*. 2005;128:2626–2644.
19. Nemy M, Cedres N, Grothe MJ, *et al*. Cholinergic white matter pathways make a stronger contribution to attention and memory in normal aging than cerebrovascular health and nucleus basalis of Meynert. *Neuroimage*. 2020;211:116607.
20. Teipel SJ, Meindl T, Grinberg L, *et al*. The cholinergic system in mild cognitive impairment and Alzheimer's disease: An in vivo MRI and DTI study. *Hum Brain Mapp*. 2011;32:1349–1362.
21. Mesulam M. The cholinergic lesion of Alzheimer's disease: Pivotal factor or side show? *Learn Mem*. 2004;11:43–49.
22. Selden NR, Gitelman DR, Salamon-Murayama N, Parrish TB, Mesulam MM. Trajectories of cholinergic pathways within the cerebral hemispheres of the human brain. *Brain*. 1998;121:2249–2257.
23. Bloem B, Poorthuis RB, Mansvelder HD. Cholinergic modulation of the medial prefrontal cortex: The role of nicotinic receptors in attention and regulation of neuronal activity. *Front Neural Circuits*. 2014;8:17.
24. Hasselmo ME. The role of acetylcholine in learning and memory. *Curr Opin Neurobiol*. 2006;16:710–715.
25. Flier WM VD, Scheltens P. Amsterdam dementia cohort: Performing research to optimize care. *J Alzheimers Dis*. 2018;62:1091–1111.
26. McKhann GM, Knopman DS, Chertkow H, *et al*. The diagnosis of dementia due to Alzheimer's disease: Recommendations from the National Institute on Aging-Alzheimer's Association workgroups on diagnostic guidelines for Alzheimer's disease. *Alzheimers Dement*. 2011;7:263–269.
27. Morris JC. The clinical dementia rating (CDR): Current version and scoring rules. *Neurology*. 1993;43:2412–2414.
28. Dubois B, Feldman HH, Jacova C, *et al*. Advancing research diagnostic criteria for Alzheimer's disease: The IWG-2 criteria. *Lancet Neurol*. 2014;13:614–629.
29. Schott JM, Lehmann M, Primativo S, *et al*. Consensus classification of posterior cortical atrophy. *Alzheimers Dement*. 2017;13:870–884.

30. Jonkman LE, de Graaf YG, Bulk M, *et al*. Normal Aging Brain Collection Amsterdam (NABCA): A comprehensive collection of postmortem high-field imaging, neuropathological and morphometric datasets of non-neurological controls. *NeuroImage Clin*. 2019;22:101698.
31. Frigerio I, Boon BDC, Lin CP, *et al*. Amyloid-β, p-tau and reactive microglia are pathological correlates of MRI cortical atrophy in Alzheimer's disease. *Brain Commun*. 2021;3:fcab281.
32. Steenwijk MD, Pouwels PJW, Daams M, *et al*. Accurate white matter lesion segmentation by k nearest neighbor classification with tissue type priors (kNN-TTPs). *Neuroimage Clin*. 2013;3:462–469.
33. Jonkman LE, Steenwijk MD, Boesen N, *et al*. Relationship between β-amyloid and structural network topology in decedents without dementia. *Neurology*. 2020;95:e532–e544.
34. Smith SM, Jenkinson M, Woolrich MW, *et al*. Advances in functional and structural MR image analysis and implementation as FSL. *Neuroimage*. 2004;23:S208–S219.
35. Tzourio-Mazoyer N, Landeau B, Papathanassiou D, *et al*. Automated anatomical labeling of activations in SPM using a macroscopic anatomical parcellation of the MNI MRI single-subject brain. *Neuroimage*. 2002;15:273–289.
36. George S, Mufson EJ, Leurgans S, Shah RC, Ferrari C, DeToledo-Morrell L. MRI-based volumetric measurement of the substantia innominata in amnestic MCI and mild AD. *Neurobiol Aging*. 2011;32:1756–1764.
37. Choi SH, Jung TM, Lee JE, Lee SK, Sohn YH, Lee PH. Volumetric analysis of the substantia innominata in patients with Parkinson's disease according to cognitive status. *Neurobiol Aging*. 2012;33:1265–1272.
38. Hepp DH, Foncke EMJ, Berendse HW, *et al*. Damaged fiber tracts of the nucleus basalis of Meynert in Parkinson's disease patients with visual hallucinations. *Sci Rep*. 2017;7:10112.
39. Cicchetti DV. Guidelines, criteria, and rules of thumb for evaluating normed and standardized assessment instruments in psychology. *Psychol Assess*. 1994;6:284–290.
40. Haselgrove JC, Moore JR. Correction for distortion of echo-planar images used to calculate the apparent diffusion coefficient. *Magn Reson Med*. 1996;36:960–964.
41. Basser PJ, Mattiello J, LeBihan D. MR diffusion tensor spectroscopy and imaging. *Biophys J*. 1994;66:259–267.
42. Basser PJ, Pierpaoli C. Microstructural and physiological features of tissues elucidated by quantitative-diffusion-tensor MRI. *J Magn Reson B*. 1996;111:209–219.
43. Li L, Rilling JK, Preuss TM, Glasser MF, Damen FW, Hu X. Quantitative assessment of a framework for creating anatomical brain networks via global tractography. *Neuroimage*. 2012;61:1017–1030.
44. Kliouevа NM, Rademaker MC, Dexter DT, *et al*. BrainNet Europe's Code of Conduct for brain banking. *J Neural Transm*. 2015;122:937–940.
45. Santos OA, Pedraza O, Lucas JA, *et al*. Ethnoracial differences in Alzheimer's disease from the FLorida Autopsied Multi-Ethnic (FLAME) cohort. *Alzheimers Dement*. 2019;15:635–643.
46. Geula C, Mesulam MM, Saroff DM, Wu CK. Relationship between plaques, tangles, and loss of cortical cholinergic fibers in Alzheimer disease. *J Neuropathol Exp Neurol*. 1998;57:63–75.
47. Al-Shaikh FS H, Duara R, Crook JE, *et al*. Selective vulnerability of the nucleus basalis of Meynert among neuropathologic subtypes of Alzheimer disease. *JAMA Neurol*. 2020;77:225–233.
48. Mesulam MM. Cholinergic circuitry of the human nucleus basalis and its fate in Alzheimer's disease. *J Comp Neurol*. 2013;521:4124–4144.
49. de Lacalle S, Iraizoz I, Ma Gonzalo L. Differential changes in cell size and number in topographic subdivisions of human basal nucleus in normal aging. *Neuroscience*. 1991;43:445–456.
50. Barnes J, Ridgway GR, Bartlett J, *et al*. Head size, age and gender adjustment in MRI studies: A necessary nuisance? *Neuroimage*. 2010;53:1244–1255.
51. Sotiropoulos SN, Zalesky A. Building connectomes using diffusion MRI: Why, how and but. *NMR Biomed*. 2019;32:e3752.
52. Benjamini Y, Hochberg Y. Controlling the false discovery rate: A practical and powerful approach to multiple testing. *J R Stat Soc Ser B*. 1995;57:289–300.
53. Thal DR, Rüb U, Orantes M, Braak H. Phases of Aβ-deposition in the human brain and its relevance for the development of AD. *Neurology*. 2002;58:1791–1800.
54. Montine TJ, Phelps CH, Beach TG, *et al*. National Institute on Aging-Alzheimer's Association guidelines for the neuropathologic assessment of Alzheimer's disease: A practical approach. *Acta Neuropathol*. 2012;123:1–11.
55. Kilimann I, Grothe M, Heinsen H, *et al*. Subregional basal forebrain atrophy in Alzheimer's disease: A multicenter study. *J Alzheimers Dis*. 2014;40:687–700.
56. Mesulam MM, Lalehzari N, Rahmani F, *et al*. Cortical cholinergic denervation in primary progressive aphasia with Alzheimer pathology. *Neurology*. 2019;92:e1580–e1588.
57. Mesulam MM. The systems-level organization of cholinergic innervation in the human cerebral cortex and its alterations in Alzheimer's disease. *Prog Brain Res*. 1996;109:285–297.
58. Muller M, Tang MX, Schupf N, Manly JJ, Mayeux R, Luchsinger JA. Metabolic syndrome and dementia risk in a multiethnic elderly cohort. *Dement Geriatr Cogn Disord*. 2007;24:185–192.
59. Caballero MÁA, Suárez-Calvet M, Duering M, *et al*. White matter diffusion alterations precede symptom onset in autosomal dominant Alzheimer's disease. *Brain*. 2018;141:3065–3080.
60. Acosta-Cabronero J, Alley S, Williams GB, Pengas G, Nestor PJ. Diffusion tensor metrics as biomarkers in Alzheimer's disease. *PLoS One*. 2012;7:e49072.
61. Stockham AL, Tievsky AL, Koyfman SA, *et al*. Conventional MRI does not reliably distinguish radiation necrosis from tumor recurrence after stereotactic radiosurgery. *J Neurooncol*. 2012;109:149–158.
62. Gold BT, Powell DK, Andersen AH, Smith CD. Alterations in multiple measures of white matter integrity in normal women at high risk for Alzheimer's disease. *Neuroimage*. 2010;52:1487–1494.
63. Etienne P, Robitaille Y, Wood P, Gauthier S, Nair NPV, Quirion R. Nucleus basalis neuronal loss, neuritic plaques and choline acetyltransferase activity in advanced Alzheimer's disease. *Neuroscience*. 1986;19:1279–1291.
64. Rinne JO, Paljärvi L, Rinne UK. Neuronal size and density in the nucleus basalis of Meynert in Alzheimer's disease. *J Neurol Sci*. 1987;79:67–76.
65. Doucette R, Fisman M, Hachinski VC, Mersky H. Cell loss from the nucleus basalis of Meynert in Alzheimer's disease. *Can J Neurol Sci*. 1986;13:435–440.
66. Arendt T, Bigl V, Tennstedt A, Arendt A. Neuronal loss in different parts of the nucleus basalis is related to neuritic plaque formation in cortical target areas in Alzheimer's disease. *Neuroscience*. 1985;14:1–14.
67. Wilcock GK, Esiri MM, Bowen DM, Hughes AO. The differential involvement of subcortical nuclei in senile dementia of Alzheimer's type. *J Neurol Neurosurg Psychiatry*. 1988;51:842–849.
68. Teipel SJ, Fritz HC, Grothe MJ. Neuropathologic features associated with basal forebrain atrophy in Alzheimer disease. *Neurology*. 2020;95:e1301–e1311.

69. Cantero JL, Atienza M, Lage C, *et al*. Atrophy of basal forebrain initiates with tau pathology in individuals at risk for Alzheimer's disease. *Cereb Cortex*. 2020;30:2083–2098.
70. Engelhardt E, Moreira DM, Laks J. Vascular dementia and the cholinergic pathways. *Dement Neuropsychol*. 2007;1:2–9.
71. Haam J, Yakel JL. Cholinergic modulation of the hippocampal region and memory function. *J Neurochem*. 2017;142:111–121.
72. Colovic MB, Krstic DZ, Lazarevic-Pasti TD, Bondzic AM, Vasic VM. Acetylcholinesterase inhibitors: Pharmacology and toxicology. *Curr Neuropharmacol*. 2013;11:315–335.
73. Herholz K, Weisenbach S, Zündorf G, *et al*. In vivo study of acetylcholine esterase in basal forebrain, amygdala, and cortex in mild to moderate Alzheimer disease. *Neuroimage*. 2004; 21:136–143.
74. Chrobak JJ, Buzsáki G. Selective activation of deep layer (V-VI) retrohippocampal cortical neurons during hippocampal sharp waves in the behaving rat. *J Neurosci*. 1994;14:6160–6170.
75. Teipel SJ, Cavedo E, Hampel H, Grothe MJ. Basal forebrain volume, but not hippocampal volume, is a predictor of global cognitive decline in patients with Alzheimer's disease treated with cholinesterase inhibitors. *Front Neurol*. 2018;9:642.
76. Leanza G. Chronic elevation of amyloid precursor protein expression in the neocortex and hippocampus of rats with selective cholinergic lesions. *Neurosci Lett*. 1998;257:53–56.
77. Garcia-Alloza M, Borrelli LA, Rozkalne A, Hyman BT, Bacskai BJ. Curcumin labels amyloid pathology in vivo, disrupts existing plaques, and partially restores distorted neurites in an Alzheimer mouse model. *J Neurochem*. 2007;102:1095–1104.
78. Ramos-Rodriguez JJ, Pacheco-Herrero M, Thyssen D, *et al*. Rapid β-amyloid deposition and cognitive impairment after cholinergic denervation in APP/PS1 mice. *J Neuropathol Exp Neurol*. 2013;72:272–285.
79. Meyer-Luehmann M, Spires-Jones TL, Prada C, *et al*. Rapid appearance and local toxicity of amyloid-β plaques in a mouse model of Alzheimer's disease. *Nature*. 2008;451:720–724.
80. MacHado A, Ferreira D, Grothe MJ, *et al*. The cholinergic system in subtypes of Alzheimer's disease: An in vivo longitudinal MRI study. *Alzheimers Res Ther*. 2020;12:51.
81. Galton CJ, Patterson K, Xuereb JH, Hodges JR. Atypical and typical presentations of Alzheimer's disease: A clinical, neuropsychological, neuroimaging and pathological study of 13 cases. *Brain*. 2000;123:484–498.
82. Dickerson BC, McGinnis SM, Xia C, *et al*. Approach to atypical Alzheimer's disease and case studies of the major subtypes. *CNS Spectr*. 2017;22:439–449.
83. Belarbi K, Burnouf S, Fernandez-Gomez F-J, *et al*. Loss of medial septum cholinergic neurons in THY-Tau22 mouse model: What links with tau pathology? *Curr Alzheimer Res*. 2011;8: 633–638.
84. Acosta-Cabronero J, Williams GB, Pengas G, Nestor PJ. Absolute diffusivities define the landscape of white matter degeneration in Alzheimer's disease. *Brain*. 2010;133:529–539.
85. Jeurissen B, Leemans A, Tournier JD, Jones DK, Sijbers J. Investigating the prevalence of complex fiber configurations in white matter tissue with diffusion magnetic resonance imaging. *Hum Brain Mapp*. 2013;34:2747–2766.
86. Huang H, Fan X, Weiner M, *et al*. Distinctive disruption patterns of white matter tracts in Alzheimer's disease with full diffusion tensor characterization. *Neurobiol Aging*. 2012;33:2029–2045.
87. Kantarci K, Murray ME, Schwarz CG, *et al*. White-matter integrity on DTI and the pathologic staging of Alzheimer's disease. *Neurobiol Aging*. 2017;56:172–179.
88. Binette AP, Theaud G, Rheault F, *et al*. Bundle-specific associations between white matter microstructure and Aβ and tau pathology in preclinical Alzheimer's disease. *eLife*. 2021;10: e62929.
89. Baldermann JC, Hardenacke K, Hu X, *et al*. Neuroanatomical characteristics associated with response to deep brain stimulation of the nucleus basalis of Meynert for Alzheimer's disease. *Neuromodulation*. 2018;21:184–190.
90. Kuhn J, Hardenacke K, Lenartz D, *et al*. Deep brain stimulation of the nucleus basalis of Meynert in Alzheimer's dementia. *Mol Psychiatry*. 2015;20:353–360.
91. Gratwicke J, Zrinzo L, Kahan J, *et al*. Bilateral nucleus basalis of Meynert deep brain stimulation for dementia with Lewy bodies: A randomised clinical trial. *Brain Stimul*. 2020;13:1031–1039.
92. Kozak LR, Bango M, Szabo M, Rudas G, Vidnyanszky Z, Nagy Z. Using diffusion MRI for measuring the temperature of cerebrospinal fluid within the lateral ventricles. *Acta Paediatr*. 2010;99: 237–243.
93. Shepherd TM, Flint JJ, Thelwall PE, *et al*. Postmortem interval alters the water relaxation and diffusion properties of rat nervous tissue - Implications for MRI studies of human autopsy samples. *Neuroimage*. 2009;44:820–826.
94. Boon BDC, Pouwels PJW, Jonkman LE, *et al*. Can post-mortem MRI be used as a proxy for in vivo? A case study. *Brain Commun*. 2019;1:fcz030.
95. Everitt BJ, Robbins TW. Central cholinergic systems and cognition. *Annu Rev Psychol*. 1997;48:649–684.
96. Kamagata K, Andica C, Hatano T, *et al*. Advanced diffusion magnetic resonance imaging in patients with Alzheimer's and Parkinson's diseases. *Neural Regen Res*. 2020;15:1590–1600.
97. Mesulam MM, Mufson EJ, Levey AI, Wainer BH. Cholinergic innervation of cortex by the basal forebrain: Cytochemistry and cortical connections of the septal area, diagonal band nuclei, nucleus basalis (substantia innominata), and hypothalamus in the rhesus monkey. *J Comp Neurol*. 1983;214:170–197.
98. Geula C, Dunlop SR, Ayala I, *et al*. Basal forebrain cholinergic system in the dementias: Vulnerability, resilience, and resistance. *J Neurochem*. 2021;158:1394–1411.
99. McAleese KE, Walker L, Erskine D, Thomas AJ, McKeith IG, Attems J. TDP-43 pathology in Alzheimer's disease, dementia with Lewy bodies and ageing. *Brain Pathol*. 2017;27:472–479.
100. Bayram E, Shan G, Cummings JL. Associations between comorbid TDP-43, Lewy body pathology, and neuropsychiatric symptoms in Alzheimer's disease. *J Alzheimers Dis*. 2019;69: 953–961.